Pyroelectric energy harvesting using Olsen cycles in purified and porous poly(vinylidene fluoride-trifluoroethylene) [P(VDF-TrFE)] thin films

2011 Smart Mater. Struct. 20 025012

(http://iopscience.iop.org/0964-1726/20/2/025012)

Smart Mater. Struct. **20** (2011) 025012 (9pp) doi:10.1088/0964-1726/20/2/025012

Pyroelectric energy harvesting using Olsen cycles in purified and porous poly(vinylidene fluoride-trifluoroethylene) [P(VDF-TrFE)] thin films

Ashcon Navid and Laurent Pilon

Mechanical and Aerospace Engineering Department, Henry Samueli School of Engineering and Applied Science, University of California, Los Angeles, CA 90095, USA

E-mail: pilon@seas.ucla.edu

Received 18 August 2010, in final form 3 December 2010
Published 14 January 2011
Online at stacks.iop.org/SMS/20/025012

Abstract

This paper is concerned with the direct conversion of heat into electricity using pyroelectric materials. The Olsen (or Ericsson) cycle was experimentally performed on three different types of 60/40 poly(vinylidene fluoride-trifluoroethylene) [P(VDF-TrFE)] copolymer samples, namely commercial, purified, and porous films. This cycle consists of two isoelectric field and two isothermal processes. The commercial and purified films were about 50 μm thick and produced a maximum energy density of 521 J l^{-1} and 426 J l^{-1} per cycle, respectively. This was achieved by successively dipping the films in cold and hot silicone oil baths at 25 and 110 °C under low and high applied electric fields of about 200 and 500 kV cm^{-1}, respectively. The 11 μm thick porous films achieved a maximum energy density of 188 J l^{-1} per cycle between 25 and 100 °C and electric field between 200 and 400 kV cm^{-1}. The performance of the purified and porous films suffered from their lower electrical resistivity and electric breakdown compared with commercial thin films. However, the energy densities of all 60/40 P(VDF-TrFE) films considered matched or exceeded those reported recently for $0.9Pb(Mg_{1/3}Nb_{2/3})O_3$–$0.10PbTiO_3$ (0.9PMN–0.1PT) (186 J l^{-1}) and $Pb(Zn_{1/3}Nb_{2/3})_{0.955}Ti_{0.045}O_3$ (243 J l^{-1}) bulk ceramics. Furthermore, the results are discussed in light of recently proposed figures of merit for energy harvesting applications.

Nomenclature

A	surface area of pyroelectric film, m^2
Bi	Biot number
b	thickness of pyroelectric film, m
C_1	capacitor capacitance, F
c_p	specific heat, J kg^{-1} K^{-1}
D	electric displacement, C m^{-2}
E	electric field, V m^{-1}
E_L	low applied electric field, V m^{-1}
E_H	high applied electric field, V m^{-1}
F_E	energy harvesting figure of merit, J m^{-3} K^{-2}
h	heat transfer coefficient, W m^{-2} K^{-1}
k^2	electrothermal coupling factor
k_f	thermal conductivity of pyroelectric film, W m^{-1} K^{-1}
L_C	characteristic length, m
N_D	energy density, J l^{-1} or J kg^{-1} per cycle
P_D	power density, W l^{-1} or W kg^{-1}
P_S	spontaneous polarization, C m^{-2}
p	pyroelectric coefficient, C m^{-2} K^{-1}
q	charge, C
R_2, R_L	resistor resistances, Ω
T	temperature, °C
T_{Curie}	Curie temperature, °C
T_{cold}	minimum temperature of pyroelectric film, °C
T_{hot}	maximum temperature of pyroelectric film, °C
T_C	temperature of cold source, °C

T_H temperature of hot source, °C
V voltage, V
V_1 voltage across capacitor C_1, V
V_2 voltage across resistor R_2, V
V_H, V_L high and low applied voltage, V
V_H^*, V_L^* high and low input voltage, V

Greek symbols

ε_0 vacuum permittivity, F m^{-1}
ε_r relative dielectric constant
ϕ porosity
ρ density, kg m^{-3}
τ cycle period, s
τ_t thermal time constant, s

Subscripts

PE refers to pyroelectric film

1. Introduction

Large amounts of waste heat are released from power, refrigeration, and heat pump cycles, as required by the second law of thermodynamics. For example, over 50% of the energy consumed by the United States in 2002 was lost typically in the form of waste heat at low temperatures [1]. Unfortunately, due to the small Carnot efficiency associated with low temperature, only a few solutions exist for harvesting low grade waste heat. Organic Rankine cycles convert thermal energy into mechanical energy at temperatures up to 200–300 °C [2]. Alternatively, Stirling engines have been used in a variety of applications including heat pumps, cryogenic refrigeration, and air liquefaction [3]. In the last several decades, thermoelectric devices have received significant attention [4]. They make use of the Seebeck effect to directly convert a steady-state temperature difference at the junction of two dissimilar metals or semiconductors into electrical energy [4]. On the contrary, pyroelectric energy conversion directly converts time-dependent temperature oscillations into electricity [5–20]. It makes use of the pyroelectric effect to create a flow of charge to or from the surface of a material as a result of successive heating and cooling. This paper experimentally investigates pyroelectric energy conversion in commercial, purified, and porous 60/40 poly(vinylidene fluoride-trifluoroethylene) [P(VDF-TrFE)] copolymer films [21].

2. Current state of knowledge

2.1. Pyroelectric materials

2.1.1. Pyroelectric effect. Pyroelectric materials possess a so-called spontaneous polarization $\mathbf{P}_S$, defined as the average electric dipole moment per unit volume in absence of an applied electric field [22]. This polarization depends strongly on temperature due to the material's crystallographic structure [23]. At steady-state ($dT/dt = 0$), the spontaneous polarization is constant. However, when the material is heated ($dT/dt > 0$), it decreases as dipole moments begin to lose their orientation. As a result, the number of charges stored at the surface of the material decreases resulting in an electric current flowing through the external circuit. When the material is cooled ($dT/dt < 0$), the dipole moments regain their orientation which increases the spontaneous polarization and allows for more charges to be stored at the surface of the material, thereby reversing the electric current flow. Some pyroelectric materials have spontaneous polarization which can be switched from $\mathbf{P}_S$ to $-\mathbf{P}_S$ by reversing the applied coercive electric field. This subclass of pyroelectric materials are called ferroelectric materials [24]. Furthermore, the relationship between electric displacement D_{PE} and electric field E_{PE} for ferroelectric materials exhibits a hysteresis curve as shown in figure 1. When the voltage is cycled across the material isothermally, the hysteresis is traveled in a counter-clockwise direction and the area enclosed by each loop represents the electrical energy dissipated. Beyond the Curie temperature, denoted by T_{Curie}, a ferroelectric material undergoes a phase transition from ferroelectric to paraelectric when the spontaneous polarization vanishes. If the phase transition occurs under a large electric field, the material will discharge a large amount of electrical energy.

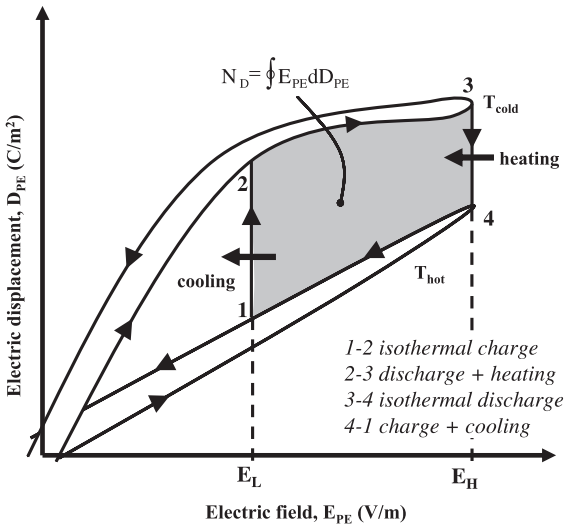

Figure 1. Electric displacement versus electric field for a typical pyroelectric material at different temperatures. The Olsen power cycle is represented by the area enclosed between 1–2–3–4.

2.1.2. Electrocaloric effect. The converse of the pyroelectric effect is the electrocaloric effect. It is the change in temperature caused by a change in applied electric field under adiabatic conditions [23]. Sebald *et al* [17] have shown theoretically that materials with large electrocaloric activity are of interest in pyroelectric energy harvesting. Large electrocaloric effects have recently been demonstrated [25–28]. For example, a temperature rise of 12 K was calculated for a change in electric field from 295 to 776 kV cm^{-1} across 350 nm thick zirconium rich $Pb(Zr, Ti)O_3$ (PZT) thin films near their Curie temperature of 220 °C [25]. Furthermore, Mischenko *et al* [26] theoretically predicted large electrocaloric activity near room temperature with 260 nm thick 0.9 $PbMg_{1/3}Nb_{2/3}O_3$–0.1$PbTiO_3$ (0.9PMN–0.1PT) thin films. The authors calculated a 5 K temperature rise as the electric field increased from 588 to 895 kV cm^{-1}

near the Curie temperature of 60 °C. Similarly, studies on 210 nm thick 0.93PMN–0.07PT films predicted a 9 K temperature rise for electric field between 0 and 723 kV cm^{-1} near 25 °C [27]. In addition a 9 K temperature rise was computed for 1 μm thick terpolymer poly(vinylidene fluoride-trifluoroethylene-chlorofluoroethylene) [P(VDF-TrFE-CFE)] films of composition 59.2/33.6/7.2 mol.% between 0 and 3000 kV cm^{-1} near 45 °C [28].

2.1.3. Figures of merit. Two figures of merit (FOMs) have been proposed to quantify the performance of pyroelectric materials for energy harvesting, namely F_E [16] and k^2 [29] defined as,

$$F_E = \frac{p^2}{\varepsilon_0 \varepsilon_r} \quad \text{and} \quad k^2 = \frac{p^2 T_H}{\rho c_p} \varepsilon_0 \varepsilon_r \qquad (1)$$

where p is the pyroelectric coefficient, $\varepsilon_0\varepsilon_r$ is the permittivity, ρ is the density, c_p is the specific heat of the pyroelectric material, and T_H is the temperature of the hot source. The figure F_E represents how much electrical power a pyroelectric material can harvest from the hot source while k^2 is a dimensionless electrothermal coupling factor representing how effectively a pyroelectric material converts thermal energy into electrical energy. Note that these figures of merit may apply to specific cycles for which they were developed.

2.1.4. Leakage current. Since pyroelectric materials are dielectric materials, their electrical resistance should ideally be infinite. In reality, however, the electrical resistance is finite and decreases as either the applied electric field or the temperature increase [11]. As a result, a so-called leakage current flows through the material, thus, reducing the electrical energy that can be harvested [10, 12, 15, 30]. Note that the energy harvesting FOMs do not account for either the pyroelectric material's electrical resistivity or the leakage current.

2.1.5. Advances in copolymer P(VDF-TrFE). Recently, efforts have been made to improve the efficiency and power density as well as to reduce the cost of pyroelectric energy conversion through the use of copolymer P(VDF-TrFE). Kouchachvili *et al* [14, 15] used a proprietary purification process for 60/40 P(VDF-TrFE) which removed approximately '0.4% of unidentifiable impurities' and resulted in 'nearly a three-fold increase in energy density'. Navid *et al* [21] experimentally synthesized porous 60/40 P(VDF-TrFE) films in order to reduce the heat capacity of the copolymer and improve its performance for energy conversion [31]. Commercial 60/40 P(VDF-TrFE) pellets were also processed as is or purified to make thin films. Full characterization of the thermophysical and electrical properties between 25 and 100 °C relevant to pyroelectric energy conversion for each type of film was reported [21]. Properties measured included (1) density, (2) ferroelectric to paraelectric phase transition temperature, (3) enthalpy of change of phase, (4) electrical resistivity, and (5) ferroelectric hysteresis, as well as (6) specific heat, (7) dielectric constant, (8) loss tangent and (9) pyroelectric coefficient as a function of temperature between 25 and 100 °C. The computed values of the figures of merit for energy harvesting F_E and k^2 indicated that the purified and porous films were attractive for thermal to electrical energy conversion.

2.2. Pyroelectric energy conversion

2.2.1. Olsen cycle—principle. Pyroelectric energy conversion using the Olsen cycle [5] (also called Ericsson cycle [17]) is achieved by alternatively placing a pyroelectric material sandwiched between two electrodes in contact with a cold and hot source, respectively at temperatures T_C and T_H, while applying the low or high electric fields E_L or E_H to perform the Olsen cycle illustrated in the D–E diagram shown in figure 1. The points 1–2–3–4 represent the electric analogue of the Olsen cycle where the enclosed area corresponds to the electrical energy produced per unit volume of material, denoted by N_D, when the electric field is cycled between E_L and E_H and the material temperature oscillates between T_{hot} and T_{cold} [9]. Furthermore, it was theoretically established that pyroelectric energy conversion using the Olsen cycle and heat regeneration can reach the Carnot efficiency between a hot and a cold thermal reservoir [8, 32]. Limitations in reaching the Carnot efficiency include (i) hysteretic and resistive losses, (ii) heat losses to the surroundings, and (iii) sensible (thermal) energy required to heat or cool the pyroelectric material [8, 32].

Moreover, Pilon and his co-workers [31, 33] numerically simulated a prototypical pyroelectric converter based on the design by Olsen *et al* [8]. Vanderpool *et al* [33] showed that the device efficiency can be increased by reducing the heat capacity of both the pyroelectric material and the working fluid while the energy and power densities can be increased by reducing the heat capacity of the pyroelectric material and increasing that of the working fluid. Navid *et al* [31] established that reducing the length of the device and the viscosity of the working fluid improved the efficiency and power density by increasing the optimum operating frequency of the device. Results showed that a maximum efficiency of 5.2% at 0.5 Hz corresponding to 55.4% of the Carnot efficiency between 145 and 185 °C can be achieved when using commercial 1.5 cSt silicone oil as the working fluid and PZST as the pyroelectric material. The associated power density was found to be 38.4 W l^{-1} of pyroelectric material at 0.5 Hz.

2.2.2. Olsen cycle—practical implementation. Successive dipping of a slab of pyroelectric material sandwiched between electrodes into cold and hot fluid baths at the specified electric fields provides a simple way to perform the Olsen cycle and to assess the energy and power generation performance of the material. For example, Olsen and co-workers performed the Olsen cycle on 70–100 μm thick 60/40 P(VDF-TrFE) thin films by successively dipping them into cold and hot 100 cSt silicone oil baths at 25 °C and 100–120 °C, respectively [11]. The low electric field E_L was kept constant at 200 kV cm^{-1} and the high electric field E_H was varied between 200 and 600 kV cm^{-1}. The maximum output energy density reported was 900 J l^{-1} of pyroelectric material per cycle at

0.125 Hz, corresponding to a power density of 112.5 W l^{-1} of pyroelectric material [11].

Ikura *et al* [12] also performed the Olsen cycle using a single 25 μm thick 60/40 P(VDF-TrFE) film subjected to periodic flow of hot and cold water at 58 and 77 °C, respectively. The low and high electric fields E_L and E_H were 40 and 480 kV cm^{-1}, respectively. The cycle time was 3.9 s and the measured energy density ranged from 15 to 52 J l^{-1}. These values were much lower than that reported by Olsen *et al* [11] due to (i) a smaller temperature swing, (ii) the temperature of the hot source was lower than the film's Curie temperature, (iii) the low electric field of 40 kV cm^{-1} might not have kept the film properly poled during process 4–1 of the Olsen cycle (figure 1), and (iv) the high electric field E_H was 480 kV cm^{-1} [12] compared with 600 kV cm^{-1} [11]. In another study, Kouchachvili and Ikura [14, 15] reported an energy density of 279 J l^{-1} per cycle by purifying 60/40 P(VDF-TrFE) synthesized using a proprietary process [14]. The electric field was cycled from 70 to 340 kV cm^{-1}. Note that the frequency, temperature range, and working fluid were not disclosed in their study [15].

More recently, Sebald *et al* [17] experimentally studied pyroelectric energy conversion in $0.9Pb(Mg_{1/3}Nb_{2/3})O_3$-$0.10PbTiO_3$ (0.9PMN–0.1PT) relaxor ceramic with Curie temperature of 60 °C [26]. A 1 mm thick 0.9PMN–0.1PT ceramic slab with its electrodes was dipped into cold and hot oil baths at 30 and 80 °C, respectively. The electric field was cycled between 0 and 35 kV cm^{-1} and the energy density obtained was 186 J l^{-1} per cycle. The authors also studied $Pb(Zn_{1/3}Nb_{2/3})_{0.955}Ti_{0.045}O_3$ relaxor single crystals for pyroelectric power generation [19]. A 1 mm thick crystal with silver paste electrodes was dipped into a cold oil bath at 100 °C and a hot oil bath with temperature ranging between 110 and 160 °C. The electric field was cycled between 0 and 20 kV cm^{-1}. A maximum energy density of 243 J l^{-1} per cycle was obtained with a cycle period of 10 s or a frequency of 0.1 Hz. Note that the maximum electric field E_H used for 0.9PMN–0.1PT and $Pb(Zn_{1/3}Nb_{2/3})_{0.955}Ti_{0.045}O_3$ was limited by the material's relatively low dielectric strength [17, 19].

This paper extends experimentally investigates Olsen pyroelectric energy conversion cycles in commercial, purified, and porous 60/40 P(VDF-TrFE) films previously synthesized and characterized [21]. In addition, the values of the energy harvesting FOMs [16, 17] were compared with experimental results to assess their relevance in estimating material performances for energy conversion.

3. Experiments and methods

3.1. Samples

The processes for preparing (i) dense films from commercial P(VDF-TrFE) pellets, (ii) purified films, and (iii) porous films used in this study were reported elsewhere [21] and need not be repeated. The process for all films began with the commercial copolymer of 60/40 P(VDF-TrFE), purchased in pellet form from Chronos Research Laboratories, Inc., San Diego, CA, USA. The commercial and purified films were approximately 50 μm thick while the porous films were about 11 μm thick. All films had a surface area of 1 cm^2. The purified and porous films had porosity ϕ equal to 16% and 33%, respectively. The Olsen cycle was performed over multiple cycles and on five different samples for each type of film. The reported energy and power densities are the averaged values over multiple cycles and the five different samples. The associated experimental uncertainties correspond to a 95% confidence interval.

The experimental apparatus required to perform the Olsen cycle consisted of a thermal and an electrical sub-system. The thermal sub-system was used to create a time-dependent temperature oscillation which heated the films to a maximum temperature T_{hot} and cooled them to a minimum temperature T_{cold}. The electrical sub-system controlled the electric field applied to the films to perform the Olsen cycle and collected the generated charges.

3.2. Thermal sub-system

A glass beaker filled with Dow Corning 200® Fluid 50 cSt silicone oil and thermally insulated was heated to temperature T_H with a hot plate and served as the hot source. Another beaker also filled with 50 cSt silicone oil was maintained at temperature T_C and served as the cold source. To ensure uniform bath temperature, the beakers were stirred and thermocouples were used to continuously monitor the baths' temperatures. To create the required time-dependent temperature oscillations, the pyroelectric films were alternately dipped into the hot and cold baths. Sufficient time (∼10 s) was allowed for the films to discharge or recharge (i.e., $\partial D_{PE}/\partial t = 0$) before the films were transferred from one bath to the other. Note that the thermal time constant needed for the films to reach the bath temperature is given by $\tau_t = \rho c_p/hb$ [34] where h is the heat transfer coefficient and b is the film thickness. It was estimated to be less than 0.3 s corresponding to $h \approx 300$ W m^{-2} K^{-1}. Note that h is typically between 10^2 and 10^3 W m^{-2} K^{-1} for convective quenching in oil baths [35]. Therefore, the P(VDF-TrFE) films reached the bath temperature very rapidly compared to the period of the Olsen cycle ensuring $T_{cold} = T_C$ and $T_{hot} = T_H$. Furthermore, the Biot number defined as $Bi = hb/k_f$ [34], where k_f is the film thermal conductivity, was calculated to be less than 0.18 indicating that the temperature is uniform across the film.

3.3. Electrical sub-system

The electrical sub-system used was the same as that used by Olsen *et al* [9]. In brief, both faces of the synthesized films were plated with aluminum electrodes and connected to the electrical circuit shown in figure 2. The circuit consisted of a Sawyer–Tower bridge [36] which measured the charge of the pyroelectric material and a resistive voltage divider placed in parallel to the Sawyer–Tower bridge to monitor the electric field applied to the material. A BK Precision Corp. model 1651 triple output DC power supply was connected to two rocker switches to provide input voltages either V_L^* and V_H^* to the Stanford Research Systems Inc. model PS325 high voltage power supply. At all times, only one switch was opened while

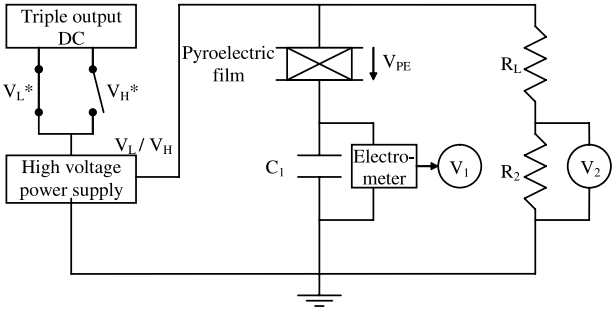

Figure 2. Electrical circuit used to perform the Olsen cycle [9].

the other was closed. The high voltage power supply amplified the input voltages V_L^* and V_H^* to output voltages V_L and V_H such that $V_L = 250V_L^*$ and $V_H = 250V_H^*$, respectively. Voltages V_L and V_H were applied to the films and synchronized with the temperature to maintain the desired low or high electric fields E_L and E_H required to perform the Olsen cycle (figure 1). Resistor R_L (7.80 MΩ) acted as a voltage divider to scale down the voltage across the resistor R_2 (21.8 kΩ) in order to match the maximum voltage input of 10 V of the data acquisition system (DAQ). The voltage V_1 was measured through a custom built electrometer to minimize the discharge of capacitor C_1 (1.0 μF) in the DAQ. The magnitude of the film electric displacement D_{PE} was defined as,

$$D_{PE} = \frac{q_{PE}}{A} = \frac{C_1 V_1}{A} \tag{2}$$

where the surface area of the film A was equal to 1 cm^2 for all films. The magnitude of the electric field across the pyroelectric film was computed via Ohm's and Kirchhoff's laws such that,

$$E_{PE} = \frac{V_{PE}}{b} = \frac{V_2(1 + R_L/R_2) - V_1}{b} \tag{3}$$

where b is the pyroelectric film's thickness.

3.4. Experimental procedure

Prior to performing the Olsen cycle, each film was poled under an applied electric field of 200 kV cm^{-1} in a 50 cSt silicone oil bath at 95 °C in order to increase the film's electrical resistivity as discussed by Navid *et al* [21]. After 230 min, the electrical resistivity of the commercial, purified, and porous films reached a steady-state value of 5.41, 2.06, and 0.75 × 10^{10} Ω m, respectively [21]. The Olsen cycle was then performed. The applied low electric field E_L was set at 200 kV cm^{-1} as suggested by Olsen *et al* [10, 11] in order to keep the films properly poled during the cooling process 1–2 in the Olsen cycle. To explore the effect of high electric field E_H on energy and power densities, E_H was varied from 300 to 600 kV cm^{-1}. To maximize the electrical energy produced, the films need to be heated above the Curie temperature, as previously discussed. Under zero applied electric field, the Curie temperatures of the commercial, purified, and porous films were similar with an average value of 66 °C [21]. The Curie temperature has been shown to increase with applied electric field and can reach ∼110 °C at 500 kV cm^{-1} [11]. Therefore, the hot source temperature T_H was set successively at 100, 110, and 120 ± 1.7 °C while the cold source was maintained at $T_C = 25 \pm 1.7$ °C.

3.5. Power generation analysis

The energy density N_D of one cycle is represented by the enclosed area within the electric displacement versus electric field (D–E) curve and is given by [7],

$$N_D = \oint E_{PE}\, dD_{PE}. \tag{4}$$

In practice, the integral was estimated numerically via the trapezoid rule. The power density, denoted by P_D, is the power generated per liter of pyroelectric material and is expressed as [7],

$$P_D = \frac{N_D}{\tau} \tag{5}$$

where τ is the cycle period taken as the time required for a film to go through one Olsen cycle on the D–E diagram.

4. Results and discussion

4.1. Power generation

4.1.1. Effect of leakage current. Figure 3 shows representative energy conversion cycles for each type of film on the D–E diagram. Here, the temperatures T_C and T_H were 25 and 100 °C, respectively. The electric fields E_L and E_H were 200 and 400 kV cm^{-1}, respectively. Note that the cycles did not start and end at the same point, i.e., points 1 and 5 did not coincide. This could be caused by irreversible material behavior. However, we speculate that the offset between points 1 and 5 corresponded to the charge conducted through the films during the entire cycle. Note that this conducted charge may 'round' the shape of processes 2–3 and 4–5 shown in figure 3. However, in the present study, these processes occurred very quickly (∼0.5 s) which limited the amount of conducted charges and therefore 'rounding'. Since the average cycle time was ∼10 s, the isoelectric field processes 1–2 and 3–4, occupy a majority of the cycle time and contribute the most to the offset. In fact, considerable leakage has been observed under constant electric field particularly for the purified and porous films [21]. The commercial films had the smallest offset, as they had the largest electrical resistivity (5.41 × 10^{10} Ω m) [21]. On the other hand, the porous films had the largest offset since they had the smallest electrical resistivity (0.75 × 10^{10} Ω m) [21]. Under these conditions, the commercial films produced the largest energy density per cycle at $N_D = 419 \pm 11$ J l^{-1}, followed by the purified films with $N_D = 346 \pm 10$ J l^{-1}, and finally the porous films with $N_D = 185 \pm 13$ J l^{-1}. Therefore, the film's electrical resistivity should be as large as possible in order to minimize the leakage current and the offset between points 1 and 5, thereby maximizing the energy density generated per cycle.

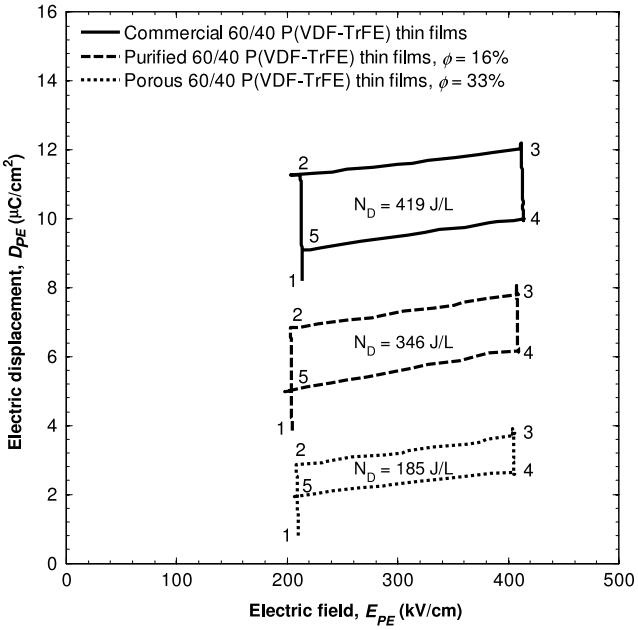

Figure 3. Representative electric displacement versus electric field diagrams for commercial, purified ($\phi = 16\%$), and porous ($\phi = 33\%$) 60/40 P(VDF-TrFE) thin films. The temperatures and electric fields were $T_C = 25\,^\circ$C, $T_H = 100\,^\circ$C, $E_L \simeq 200$ kV cm^{-1}, and $E_H \simeq 400$ kV cm^{-1}.

4.1.2. Effect of high applied electric field and hot source temperature. Figure 4 summarizes the energy and power densities generated by the commercial, purified, and porous films for T_H between 100 and 120 °C and E_H ranging from 300 to 600 kV cm^{-1}. The energy density N_D and power density P_D reported in figure 4 represent the averaged values over 5 samples themselves averaged over 5 cycles for each sample type. The measurements were repeatable from cycle to cycle and from one film to another film. Figure 4 indicated that for a given hot source temperature T_H, the energy and power densities increased as a function of the high applied field E_H up to 500 kV cm^{-1} for the commercial and purified films and up to 400 kV cm^{-1} for the porous films. Indeed, raising E_H increased the electric field span (E_H–E_L) in the Olsen cycle which increased the energy and power densities as suggested by equations (4) and (5). However, for the commercial films, the energy and power densities decreased beyond $E_H = 500$ kV cm^{-1} due to a significant increase in leakage current. Note that the purified films experienced dielectric breakdown at applied electric fields greater than 500 kV cm^{-1} while the porous films broke down at E_H greater than 400 kV cm^{-1} and temperatures larger than 100 °C due to the presence of pores which reduces the films' dielectric strength [21].

Moreover, the commercial 60/40 P(VDF-TrFE) films produced the largest energy and power densities per unit volume for all values of T_H and E_H explored. The larger electrical resistivity of the commercial films minimized leakage current, thus maximizing the generated electrical energy and power. When the hot source temperature T_H was raised from 100 to 110 °C, both the energy and power densities at a given high applied electric field E_H increased. Indeed, the Curie temperature of 60/40 P(VDF-TrFE) for E_H between 300 and 600 kV cm^{-1} ranges from approximately 90 to 110 °C [11]. Therefore, raising T_H allowed the commercial films to undergo ferroelectric to paraelectric phase transition which further discharged the films. However, larger values of T_H reduced the energy density due to an increase in leakage current.

The energy and power densities generated per unit volume of purified films were smaller than those generated by the commercial films for all values of T_H and E_H. Indeed, the performance of the purified films suffered from their lower electrical resistivity which resulted in larger leakage current. However, the purified films produced similar energy and power densities as the commercial films on a per unit mass basis for $T_H = 100$ and 110 °C thanks to the presence of pores which reduced their density. In fact, the energy density per unit mass for the purified films was about 25% greater than that of the commercial films at $T_H = 100\,^\circ$C and $E_H = 300$ kV cm^{-1}. However, when T_H reached 120 °C, the leakage current of the purified films increased so much that the energy and power densities per unit volume and per unit mass were smaller than those of the commercial films' for all values of E_H.

The cycle period τ for the commercial and purified films depended on T_H but was independent of E_H. Moreover, τ was about the same for both types of films. It decreased from 12.1 ± 1.0 s to 10.0 ± 0.6 s and 7.6 ± 0.8 s as the temperature T_H increased from 100 °C to 110 °C and 120 °C, respectively. Indeed, the heating and cooling rates experienced by the films as they were dipped between the cold and hot sources increased when the hot source temperature was raised.

The porous films had the smallest energy and power densities per unit volume and per unit mass for all experimental conditions explored due to their much smaller electrical resistivity responsible for excessive leakage current. In addition, the introduction of pores reduced the dipole moment per unit volume, corresponding to a decrease in pyroelectric coefficient [21] which further limited the electrical energy the films could produce. The cycle period of the porous films was also independent of high applied electric field E_H and equal to 9.9 ± 0.7 s for $T_H = 100\,^\circ$C. This was about 18% less than that of the commercial and purified films at the same temperature. Indeed, the 11 μm thick porous films had smaller time constant τ_t because they were about five times thinner and their heat capacity was 42 and 19% smaller than that of the commercial and purified films, respectively [21].

4.1.3. Maximum energy and power densities. The largest energy density achieved by the commercial films was 521 ± 19 J l^{-1} or 278 ± 10 J kg^{-1} per cycle, corresponding to a power density of 51 ± 2 W l^{-1} or 27 ± 1 W kg^{-1} for $T_C = 25\,^\circ$C, $T_H = 110\,^\circ$C, $E_L = 200$ kV cm^{-1}, and $E_H = 500$ kV cm^{-1}. The maximum energy and power densities for the purified films were also achieved under the same conditions and were found to be $N_D = 426 \pm 20$ J l^{-1} or 270 ± 13 J kg^{-1} per cycle and $P_D = 45 \pm 4$ W l^{-1} or 28 ± 3 W kg^{-1}. Finally, the porous films achieved a maximum energy density of 188 ± 13 J l^{-1} or 150 ± 11 J kg^{-1} per cycle and a maximum power density of 18 ± 1 W l^{-1} or 15 ± 1 W kg^{-1} for $T_C = 25\,^\circ$C, $T_H = 100\,^\circ$C, $E_L = 200$ kV cm^{-1}, and $E_H = 400$ kV cm^{-1}.

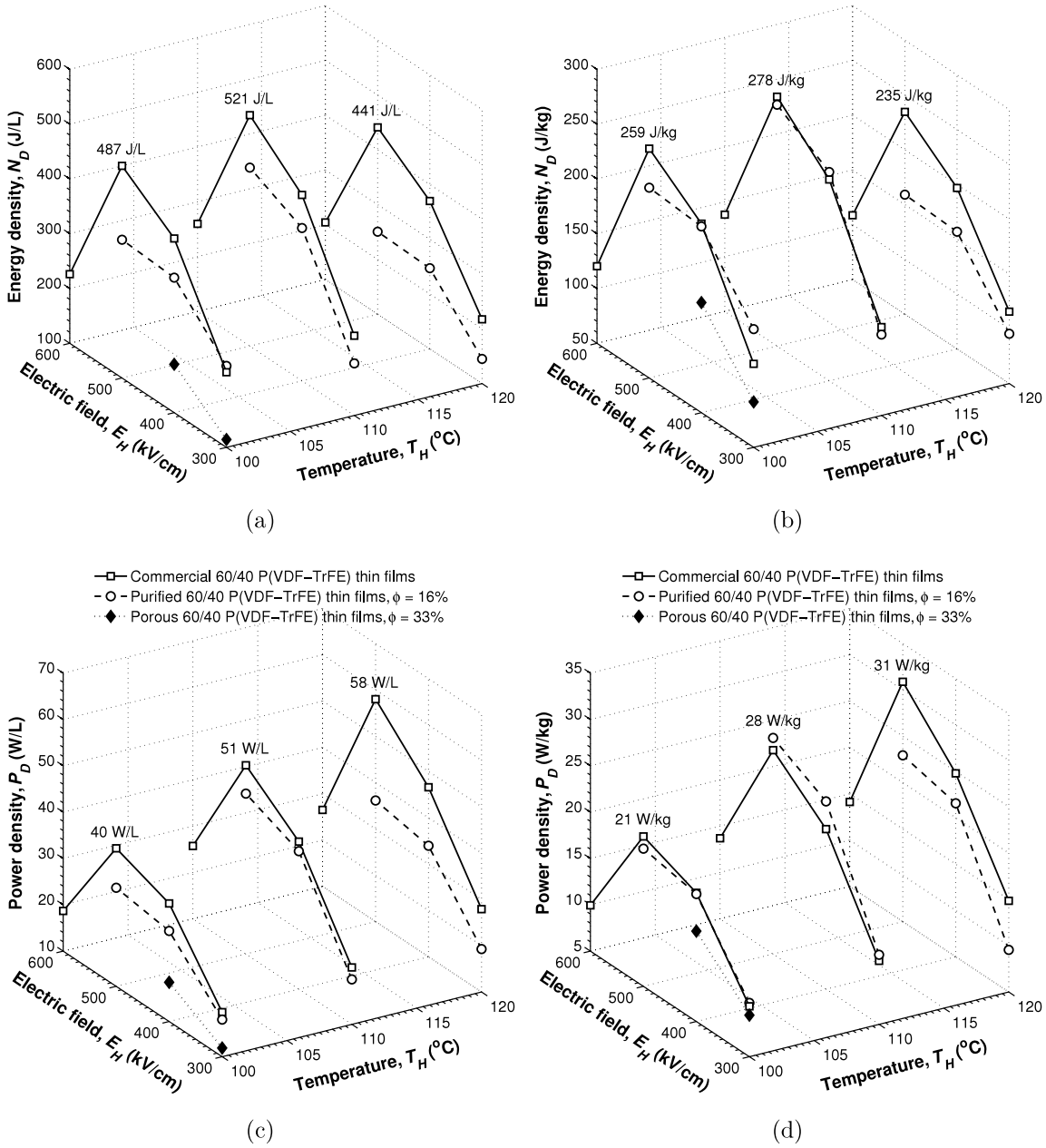

Figure 4. Energy density N_D (a) per unit volume and (b) per unit mass and power density P_D (c) per unit volume and (d) per unit mass as a function of electric field E_H and temperature T_H for commercial, purified ($\phi = 16\%$), and porous ($\phi = 33\%$) 60/40 P(VDF-TrFE) thin films [21]. The electric field E_L and temperature T_C were 200 kV cm^{-1} and 25 °C, respectively.

4.2. Discussion

The energy densities of the commercial and purified films were more than twice as large as those reported for 0.9PMN–0.1PT ceramics [17] and $Pb(Zn_{1/3}Nb_{2/3})_{0.955}Ti_{0.045}O_3$ single crystals [19]. The much larger dielectric strength of the P(VDF-TrFE) films [11] enabled the use of larger electric field E_H resulting in a larger field span (E_H–E_L) in the Olsen cycle and increasing the energy density as suggested by equation (4). Note that P(VDF-TrFE) can be made in different compositions, however, only those containing more than 50% VDF exhibit a ferroelectric to paraelectric phase transition [37] and are of interest for pyroelectric energy conversion [11].

The figure of merit F_E for the commercial, purified, and porous films was respectively reported to be 7.93, 10.17, and 5.24 J m^{-3} K^{-2} near room temperature [21]. For the purified films, F_E was greater than that of the commercial films due to their larger pyroelectric coefficient. However, F_E for the porous films was the smallest due to their smaller pyroelectric coefficient. This suggests that the purified films should produce the most electrical power. Experimentally, however, the commercial films produced the largest power due to their larger electrical resistivity which minimized the leakage current.

Moreover, the electrothermal coupling factor k^2 was found to be 0.93, 1.68, and 1.06 × 10^{-3} near room temperature for

the commercial, purified, and porous films, respectively [21]. The larger value of k^2 for the purified and porous films was due to the reduction in their heat capacity ρc_p and to the larger pyroelectric coefficient of the purified films. Here also, the values of k^2 suggest that purified and porous films should perform better than commercial films. However, this was not observed experimentally. Note that the above FOMs were developed assuming linear material behavior subjected to small temperature and field changes [16, 29]. To maximize the energy harvested, large changes in displacement, electric field, and temperature are necessary but they result in nonlinear material behavior. Furthermore, to maximize the performance of Olsen cycles, the films should be heated beyond their Curie temperatures. Note that the pyroelectric coefficient is zero above T_{Curie} [21], which corresponds to $F_E = k^2 = 0$. Thus, new FOMs to rapidly compare materials or models for predicting the energy density harvesting using Olsen cycles should be developed. One possible method could make use of electrocaloric measurements as discussed by Sebald *et al* [17].

5. Conclusion

This work aimed at experimentally investigating pyroelectric energy harvesting using Olsen (Ericsson) cycle on commercial, purified, and porous 60/40 P(VDF-TrFE) thin films previously prepared and characterized [21]. It was established that the commercial films produced the largest energy density of 521 ± 19 J l^{-1} or 278 ± 10 J kg^{-1} per cycle, corresponding to a power density of 51 ± 2 W l^{-1} or 27 ± 1 W kg^{-1} for $T_C = 25\,^\circ$C, $T_H = 110\,^\circ$C, $E_L = 200$ kV cm^{-1}, and $E_H = 500$ kV cm^{-1}. The performance of purified films was negatively affected by leakage current at high temperature. In addition, porous films showed poor performances due to their low electrical resistivity and dielectric strength. The electrical resistivity was found to have a significant impact on the films' performance and should ideally be made as large as possible.

Moreover, the energy harvesting figure of merit F_E had predicted that the purified films would perform better since they had the largest pyroelectric coefficients. However, experimentally, the commercial films produced the greatest power as they had the largest electrical resistivity resulting in smaller leakage current. The maximum energy density of the commercial films was found to be nearly three times larger than that of 0.9PMN–0.1PT [17] and about twice as large as that reported for $Pb(Zn_{1/3}Nb_{2/3})_{0.955}Ti_{0.045}O_3$ [19]. The results indicated that 60/40 P(VDF-TrFE) is a promising material for pyroelectric energy harvesting. Future work should focus on further improving its dielectric strength and electrical resistivity. Finally, new figures of merit taking into consideration the material electrical resistivity and dielectric strength should be defined as both of these properties were found to be important.

Acknowledgments

This work was funded by the Office of Naval Research under Award N000140710671 (Program Manager: Dr Mark Spector). The authors would like to thank Dr R B Olsen for useful discussions and exchange of information.

References

[1] Lawrence Livermore National Laboratory. US energy flow trends-2002 2008 http://eed.llnl.gov/flow
[2] Liu B T, Chien K H and Wang C C 2004 Effect of working fluids on organic Rankine cycle for waste heat recovery *Energy* **29** 1207–17
[3] Thombare D G and Verma S K 2008 Technological development in the Stirling cycle engines *Renew. Sustain. Energy Rev.* **12** 1–38
[4] Riffat S B and Ma X 2003 Thermoelectrics: a review of present and potential applications *Appl. Therm. Eng.* **23** 913–35
[5] Olsen R B, Bruno D A, Briscoe J M and Butler W F 1981 A pyroelectric energy converter which employs regeneration *Ferroelectrics* **38** 975–8
[6] Olsen R B 1982 Ferroelectric conversion of heat to electrical energy—a demonstration *J. Energy* **6** 91–5
[7] Olsen R B and Brown D D 1982 High-efficiency direct conversion of heat to electrical energy related pyroelectric measurements *Ferroelectrics* **40** 17–27
[8] Olsen R B, Bruno D A and Briscoe J M 1984 Cascaded pyroelectric energy converter *Ferroelectrics* **59** 205–19
[9] Olsen R B, Bruno D A and Briscoe J M 1985 Pyroelectric conversion cycles *J. Appl. Phys.* **58** 4709–16
[10] Olsen R B, Bruno D A and Briscoe J M 1985 Pyroelectric conversion cycle of vinylidene fluoride-trifluoroethylene copolymer *J. Appl. Phys.* **57** 5036–42
[11] Olsen R B and Bruno D A 1986 Pyroelectric conversion materials *Proc. 21st Intersociety Energy Conversion Engineering Conf. (San Diego, CA, Aug. 1986)* (Washington, DC: American Chemical Society) pp 89–93
[12] Ikura M 2002 Conversion of low-grade heat to electricity using pyroelectric copolymer *Ferroelectrics* **267** 403–8
[13] Kouchachvili L and Ikura M 2006 High performance pyroelectric converter *Proc. 6th IASTED Int. Conf. European Power and Energy Systems (Rhodes, June 2006)* pp 366–71
[14] Kouchachvili L and Ikura M 2006 High performance P(VDF-TrFE) copolymer for pyroelectric conversion *US Patent Specification* 7,323,506
[15] Kouchachvili L and Ikura M 2008 Improving the efficiency of pyroelectric conversion *Int. J. Energy Res.* **32** 328–35
[16] Sebald G, Seveyrat L, Guyomar D, Lebrun L, Guiffard B and Pruvost S 2006 Electrocaloric and pyroelectric properties of $0.75Pb(Mg_{1/3}Nb_{2/3})O_3$–$0.25PbTiO_3$ single crystals *J. Appl. Phys.* **100** 124112
[17] Sebald G, Pruvost S and Guyomar D 2008 Energy harvesting based on Ericsson pyroelectric cycles in a relaxor ferroelectric ceramic *Smart Mater. Struct.* **17** 015012
[18] Guyomar D, Pruvost S and Sebald G 2008 Energy harvesting based on FE–FE transition in ferroelectric single crystals *IEEE Trans. Ultrason. Ferroelectr. Freq. Control* **55** 279–85
[19] Khodayari A, Pruvost S, Sebald G, Guyomar D and Mohammadi S 2009 Nonlinear pyroelectric energy harvesting from relaxor single crystals *IEEE Trans. Ultrason. Ferroelectr. Freq. Control* **56** 693–9
[20] Nguyen H, Navid A and Pilon L 2010 Pyroelectric energy converter using co-polymer P(VDF-TrFE) and Olsen cycle for waste heat energy harvesting *Appl. Therm. Eng.* **30** 2127–37
[21] Navid A, Lynch C S and Pilon L 2010 Purified and porous poly(vinylidene fluoride-trifluoroethylene) [P(VDF-TrFE)] thin films for pyroelectric infrared sensing and energy harvesting *Smart Mater. Struct.* **19** 055006
[22] Lang S B 1974 *Sourcebook of Pyroelectricity* (New York: Gordon and Breach)
[23] Lang S B 2005 Pyroelectricity: from ancient curiosity to modern imaging tool *Phys. Today* **58** 31–6

[24] Lang S B and Das-Gupta D K 2001 *Handbook of Advanced Electronic and Photonic Materials and Devices* vol 4 (San Diego, CA: Academic)

[25] Mischenko A S, Zhang Q, Scott J F, Whatmore R W and Mathur N D 2006 Giant electrocaloric effect in thin-film $PbZr_{0.95}Ti_{0.05}O_3$ *Science* **311** 1270–1

[26] Mischenko A S, Zhang Q, Whatmore R W, Scott J F and Mathur N D 2006 Giant electrocaloric effect in the thin film relaxor ferroelectric 0.9 $PbMg_{1/3}Nb_{2/3}O_3$–0.1$PbTiO_3$ near room temperature *Appl. Phys. Lett.* **89** 242912

[27] Correia T M, Young J S, Whatmore R W, Scott J F, Mathur N D and Zhang Q 2009 Investigation of the electrocaloric effect in a $PbMg_{2/3}Nb_{1/3}O_3$–$PbTiO_3$ relaxor thin film *Appl. Phys. Lett.* **95** 182904

[28] Neese B, Lu S G, Chu B and Zhang Q M 2009 Electrocaloric effect of the relaxor ferroelectric poly(vinylidene fluoride-trifluoroethylene-chlorofluoroethylene) terpolymer *Appl. Phys. Lett.* **94** 042910

[29] Sebald G, Lefeuvre E and Guyomar D 2008 Pyroelectric energy conversion: optimization principles *IEEE Trans. Ultrason. Ferroelectr. Freq. Control* **55** 538–51

[30] Kouchachvili L and Ikura M 2006 Pyroelectric conversion-effects of P(VDF-TrFE) preconditioning on power conversion *J. Electrost.* **65** 182–8

[31] Navid A, Vanderpool D, Bah A and Pilon L 2010 Towards optimization of a pyroelectric energy converter for harvesting waste heat *Int. J. Heat Mass Transfer* **53** 4060–70

[32] Gonzalo J A 1976 Ferroelectric materials as energy converters *Ferroelectrics* **11** 423–30

[33] Vanderpool D, Yoon J H and Pilon L 2008 Simulations of a prototypical device using pyroelectric materials for harvesting waste heat *Int. J. Heat Mass Transfer* **51** 5052–62

[34] Incropera F P and DeWitt D P 2002 *Heat and Mass Transfer* (New York: Wiley)

[35] Liščić B 2009 Heat transfer control during quenching *Mater. Manuf. Process.* **24** 879–86

[36] Sawyer C B and Tower C H 1930 Rochelle salt as a dielectric *Phys. Rev.* **35** 269–75

[37] Davis G T, Broadhurst M G, Lovinger A J and Furukawa T 1984 Hysteresis in copolymers of vinylidene fluoride and trifluoroethylene *Ferroelectrics* **57** 73–84